Binary-electron emission in grazing ion-surface collisions

M. L. Martiarena,* E. A. Sánchez,* O. Grizzi,* and V. H. Ponce
Centro Atómico Bariloche, 8400 Bariloche, Rio Negro, Argentina
(Received 5 July 1995)

We study the binary-electron production due to single-electron excitation by the direct screened Coulomb interaction between the projectile and the surface. We analyze the energy spectra of electrons emitted during the interaction of ions with surfaces under grazing incidence conditions. For high ion energies (>100 keV/amu), the binary-electron peak is shifted to energies lower than those expected in ion-gas collisions. The calculations of the electron energy distributions for different projectile charges, surfaces with different Fermi energies and work functions, and several electron observation angles are in qualitative agreement with the experimental data. For lower ion energies (30–100 keV), the present model gives a better description at large observation angles. This indicates that the ''shifted convoy'' structure, which dominates the electron emission spectrum around the direction of the specular reflection, cannot be ascribed to a binary-collision mechanism.

PACS number(s): 34.50.Dy, 79.20.−m

I. INTRODUCTION

The angle and energy distributions of electrons emitted during the scattering of fast grazing ions from surfaces have been the subject of intense research during the past years. The electron spectra have specific characteristics that depend on the projectile energy and incidence angle, on the electron observation angle, and on the chemical and topographic compositions of the surface.

The electron energy distribution presents a maximum between 3 and 9 eV that increases and shifts to lower electron energies for increasing observation angles [1–4]. At electron energies around $E_{\mathrm{CE}}=m_e v_p^2/2$ (with v_p the projectile velocity and m_e the electron mass) and observation angles close to the direction of the ion specular reflection, other structures have been reported whose shape and energy position depend on the surface topography [5]. For rough surfaces a strong structure is observed at E_{CE}, usually referred to as the convoy electron peak (CEP) E_{CE}. For relatively flat surfaces, besides the convoy peak, a broader structure at $E_M > E_{\mathrm{CE}}$ can be observed. For sufficiently smooth surfaces and low electron observation angles, the last structure becomes the dominant feature of the electron spectrum while the CEP disappears in the background. For this case, the low electron energy structure (between 3 and 9 eV) becomes much smaller than that observed for rough surfaces.

The structure at E_M, associated with flat surfaces, has been observed for projectile velocities ranging from $v_p \leqslant v_F$ (v_F is the Fermi velocity) [5–7] up to v_P of several atomic units [8–10]. Its dependence with experimental parameters has been investigated in several works; on the other hand, its theoretical description [11,12] is still in its beginnings and a detailed comparison with the whole range of experimental results has not, as far as we know, been done. In particular, for the low projectile energy range the structure at E_M has been attributed to a binary encounter process [6,7].

At electron energies higher than E_M, a broad structure can be observed, which has been identified as a binary peak (BP). This structure is well known in ion-gas collisions [13–16]. The BP comes from hard collisions between the impinging ion and target electrons. From energy and momentum conservation in the projectile-electron subsystem, it is possible to estimate the position of the binary peak as $k_f = 2v_p \cos(\theta)$ (k_f is the final electron momentum and θ the electron emission angle). In the spectra published by Kimura *et al.* [10,17], Koyama [9], and Ishikawa *et al.* [18] the maxima of the binary structures observed close to the direction of the ion specular reflection appear centered at electron energies lower than $2v_p^2$, i.e., the expected value of the maximum in a binary-encounter collision. A similar energy shift of the binary peak has also been observed in ion-gas collisions [16]; however, the energy shift in this case is smaller than that observed in ion-surface interactions.

For particular experimental conditions, i.e., energy and incidence angle of the projectile, electron observation angle, and surface topography, it is possible to observe the low-energy peak, the convoy electron peak, the peak at E_M, and the binary peak all coexisting in the same spectrum [9]. In the present work we study the contributions to the electron spectrum coming from single-electron excitation produced by the screened Coulomb interaction between the incident ion and the surface electrons (the binary contribution). We analyze these contributions for high projectile energies (> 100 keV) as a function of (a) the mass and charge of the projectile, (b) the surface properties (Fermi energy and work function), and (c) the electron observation angle. The present theoretical model gives a reasonable description of the experimental data.

In the case of low projectile energy (30–100 keV) we compare the behavior of the binary structure and the structure at E_M. The comparison between calculation and experimental data taken in our laboratory suggests that it is not possible to describe the structure at E_M as a binary peak.

II. THEORETICAL MODEL

We calculate the electron energy distribution resulting from the bulk electron ionization [3,4,19] produced by the

*Also at Consejo Nacional de Investigaciones Científicas y Técnicas, Argentina.

direct ion-electron screened Coulomb interaction, approximated by a Yukawa-type potential. We consider grazing incidence and describe the solid within the jellium approximation. The electrons are considered essentially free within the metal volume V, but bound to the metal half space by a potential step $V_0=E_F+W$, where E_F is the Fermi energy and W the work function. Solutions of the Schrödinger equation for this potential can be written as

$$\Psi_{\vec{k}}^{j}(\vec{r})=\frac{e^{-i\vec{k}_{||}\cdot\vec{R}}}{\sqrt{2\pi A}}\varphi_{k_z}^{j}(z), \tag{1}$$

where $\vec{r}=(\vec{R},\vec{z})$, $\vec{k}=(\vec{k}_{||},\vec{k}_z)$, and A is the surface area, with states

$$\varphi_{k_{iz}}^{0}(z)=\begin{cases}\dfrac{k_{iz}-i\gamma}{k_{iz}+i\gamma}e^{-ik_{iz}z}+e^{ik_{iz}z}, & z<0\\[2ex] \dfrac{2k_{iz}}{k_{iz}+i\gamma}e^{-\gamma z}, & z>0\end{cases} \tag{2}$$

confined along the direction normal to the surface. The free states are separated in two orthogonal sets: outgoing waves

$$\varphi_{k_{fz}}^{+}(z)=\begin{cases}\dfrac{p-k_{fz}}{k_{fz}+p}e^{-ipz}+e^{ipz}, & z<0\\[2ex] \dfrac{2p}{k_{fz}+p}e^{ik_{fz}z}, & z>0\end{cases} \tag{3}$$

and incoming waves

$$\varphi_{k_{fz}}^{-}(z)=\sqrt{\frac{p}{k_{fz}}}\begin{cases}\dfrac{2k_{fz}}{k_{fz}+p}e^{-ipz}, & z<0\\[2ex] \dfrac{k_{fz}-p}{k_{fz}+p}e^{ik_{fz}z}+e^{-ik_{fz}z}, & z>0,\end{cases} \tag{4}$$

with $p=\sqrt{2V_0+k_{fz}}$ and $\gamma=\sqrt{2V_0-k_{iz}}$.

The transport of the emitted electrons (up to the surface) is included through an exponential factor e^{qz} that multiplies the electron final states inside the solid $q\propto 1/\lambda$, with λ the electron mean free path. This takes into account the electron loss due to multiple collisions only in the outgoing trajectory.

We assume that the ion moves along a classical trajectory

$$\vec{R}(t)=B\vec{e}_z+t\vec{v}_{p\pm},$$

with $\vec{v}_{p\pm}=v_{\parallel}\vec{e}_x\pm v_{\perp}\vec{e}_z$, where $-$ and $+$ correspond to the incoming ($t<0$) and outgoing ($t>0$) parts of the trajectory, respectively. B is the distance of closest approach with respect to the jellium edge (located at $z=0$). The Fourier transform of the screened Coulomb field of the impinging ion is

$$\Phi(\vec{Q}_{||},z,t)=2\pi Z_p^2\frac{e^{i\vec{v}_{||}\cdot\vec{Q}_{||}t}}{(\vec{Q}_{||}^{\,2}+a^2)^{1/2}}e^{-|\beta||\vec{Q}_{||}|}, \tag{5}$$

with $\vec{Q}_{||}=\vec{k}_{i||}-\vec{k}_{f||}$ the transferred parallel momentum, $\beta=z\pm v_{\perp}t+B$, and a the Yukawa screening parameter. Using the method of variation of parameters for the case of target ionization, the perturbed wave function describing the possible states of the system at time t may be written as [20]

$$\begin{aligned}\Delta\Psi(\vec{r},t)=&\frac{1}{2\pi^3\sqrt{A}}\int d\omega\int d\vec{k}_{f||}e^{-i\vec{k}_{f||}\cdot\vec{R}}e^{-i(\epsilon_0+\omega)t}\\ &\times\sum_{\sigma=\pm}\int_0^{\infty}dk_{fz}\varphi_{k_{fz}}^{j}(z)\frac{e^{-i(\epsilon_f-\epsilon_0-\omega)(t-t_0)}-1}{\epsilon_f-\epsilon_0-\omega}\\ &\times\langle\varphi_{k_{fz}}^{j}|\Phi(\vec{Q}_{||},z,\omega)|\varphi_{k_{iz}}^{0}\rangle.\end{aligned}$$

We must consider the asymptotic wave functions describing the final states of the excited electrons. Following the method developed by Bethe and applying it to the ion-surface interaction, the perturbed wave function may be approximated by [21]

$$\begin{aligned}\Delta\Psi(\vec{r},t)=&\frac{1}{\sqrt{2\pi A}}\int\int d\vec{k}_f e^{-i\vec{k}_f\cdot\vec{r}}e^{-i\epsilon_f t}\theta(k_{fz}(t-t_0)-z)\\ &\times\mathbf{M}_{\vec{k}_f\leftarrow\vec{k}_i},\end{aligned} \tag{6}$$

where θ is the unit step function and

$$\begin{aligned}\mathbf{M}_{\vec{k}_f\leftarrow\vec{k}_i}=&\frac{-i}{(2\pi)^2}\left(\frac{k_{fz}}{k_{fz}+p}\right)\Bigg[2\langle\varphi_{k_{fz}}^{+}|\Phi(\vec{Q}_{||},z,\omega)|\varphi_{k_{iz}}^{0}\rangle\\ &+\frac{k_{fz}-p}{\sqrt{k_{fz}p}}\langle\varphi_{k_{fz}}^{-}|\Phi(\vec{Q}_{||},z,\omega)|\varphi_{k_{iz}}^{0}\rangle\Bigg]\end{aligned} \tag{7}$$

represents the transition amplitude. The electron emission probability is obtained by integration of the transition amplitude over the initial momentum distribution inside the Fermi sphere of radius $k_F=\sqrt{2E_F}$

$$P(k_{fz},\vec{k}_{f||})=\int_{\vec{k}\le\vec{k}_F}d\vec{k}\rho(\epsilon_0)|\mathbf{M}_{\vec{k}_f\leftarrow\vec{k}_i}|^2. \tag{8}$$

We evaluate $\mathbf{M}_{\vec{k}_f\leftarrow\vec{k}_i}$ analytically and the emission probability numerically considering parallel ion trajectories.

III. EXPERIMENTAL SETUP

The experiments at low projectile energies were performed in an UHV chamber that has been described previously [22]. The mass-analyzed ion beam is generated in a radio-frequency source, accelerated to 30–100 keV and collimated to a spot size of $\phi\approx 1.5$ mm diameter with an angular divergence of $\sim 0.2°$. The Al(111) target was mechanically polished with 0.05 μm alumina and cleaned *in situ* by repeated cycles of grazing 20 keV Ar bombardment and 5 min of annealing at 500 °C. No contaminants were detected after the cleaning cycles. The electrons were angular and energy analyzed by a custom made rotatable cylindrical mirror analyzer working at 1% energy resolution and 2° angular resolution. The electron spectra were corrected by the transmission function of the analyzer and normalized to the incident ion current (measured in a Faraday cup after removing the sample from the ion beam path).

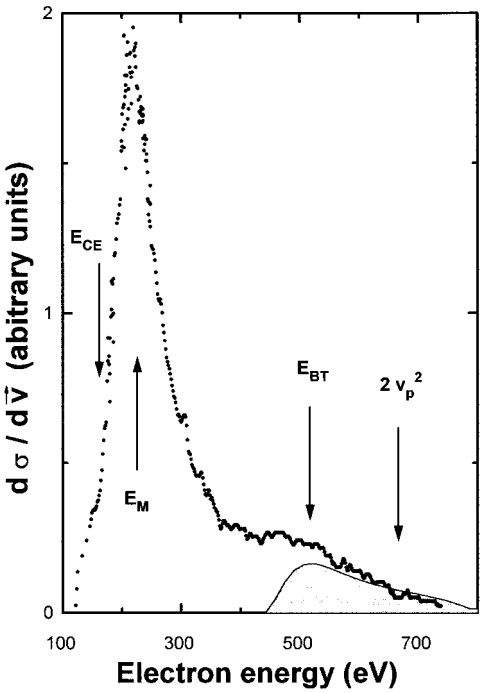

FIG. 1. Electron emission spectrum $d\sigma/d\vec{v}$ for 2.1 MeV Li^+ impinging on a SnTe surface with $\theta_i = 0.34°$ and $\theta_0 = 6.3°$. The dark region corresponds to the calculation and the points to the experimental data extracted from Kimura *et al.* [10]. The arrows indicate the convoy electron energy E_{CE}, the maximum of the electron distribution at E_M, the theoretical binary peak maximum E_{BT}, and $2v_p^2$. The height of the calculated spectrum was chosen arbitrarily.

IV. RESULTS AND DISCUSSION

Although the interaction potential described here is a simple approximation to the potential generated by the ion close to the surface, the calculation allows us to study the main features of the binary-electron distribution and its dependence with the projectile energy and charge, the Fermi energy and work function of the target, and the electron observation angle.

The spatial attenuation of the final electron states in the solid, considered through the factor e^{qz}, seems not to affect the emission probability very much. This has been discussed extensively in Ref. [4]. For simplicity we use $q = 0.01$ a.u. in all the calculations.

In order to give an idea of the principal characteristics of the binary peak in the high projectile energy regime, we present in Fig. 1 both the experimental results extracted from Kimura *et al.* [10] and our calculation for 2.1 MeV Li^+ impinging on a SnTe surface. In the calculation the surface was characterized by a Fermi energy of 12.54 eV and a work function of 4.7 eV. The incidence angle θ_i was set to 0.34° and the observation angle θ_0 to 6.3°, both defined with respect to the surface plane.

We observe in the experimental spectrum that the structure at E_M is clearly separated from the calculated binary peak. Furthermore, the binary-peak maximum is shifted to an energy around $E_{BT} = 520$ eV, considerably lower than $2v_p^2 = 660$ eV.

The maximum electron energy of kinetically emitted electrons is determined by the relative electron-ion velocity, the work function, and the Fermi energy. The maximum momentum transferred to the electrons inside the solid through a binary-encounter interaction is equal to $v_p + k_F$ (in the projectile frame). Those electrons that can overcome the surface barrier will be refracted, losing an amount of energy equal to the work function of the surface. Therefore, the maximum momentum of the electron outside the solid, evaluated in the laboratory frame for $\theta_0 \approx \theta_i$, is [19]

$$k_f^M = |\vec{v}_p + \vec{k}_F| - \sqrt{2W} + v_{p||} . \tag{9}$$

The detailed shape and position of the maximum (E_{BT}) of the BP depend also on the density of states of the solid. In the present work we have considered a free-electron density of states within the Fermi sphere $\rho(k_i) = k_i$. A thorough evaluation of the BP should take into account a more realistic description of the density of states and the surface potential barrier; however, this approximation gives reasonable agreement with the observed binary structure, with $E_{BT} < 2v_p^2$.

A. The binary structure for high projectile energies

For high projectile energies we study the dependence of the BP with different experimental parameters.

1. Mass and charge of the projectile

We show in Fig. 2 the electron emission probability $d\sigma/d\vec{v}$ calculated for 0.3 MeV/amu H^+, He^+, Li^+, and C^{2+} ions scattering from a SnTe surface with $\theta_i = 0.34°$ and $\theta_0 = 5.73°$.

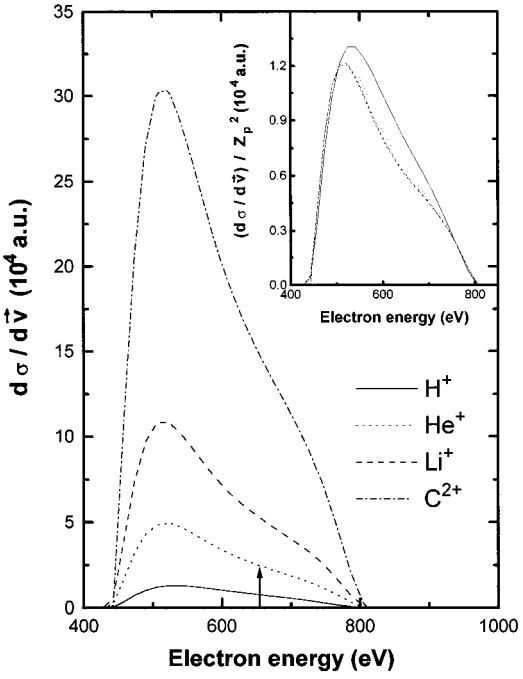

FIG. 2. Electron emission probability $d\sigma/d\vec{v}$ calculated for 0.3 MeV/amu H^+, He^+, Li^+, and C^{2+} ions scattering from a SnTe surface with $\theta_i = 0.34°$ and $\theta_0 = 5.73°$. The inset shows $d\sigma/d\vec{v}$ divided by Z_p^2. The arrow indicates the energy $2v_p^2$.

The intensity of the BP is mainly determined by Z_p^2, as can be observed in the inset of Fig. 2, where we present $d\sigma/d\vec{v}$ divided by Z_p^2. This dependence comes from the use of the first Born approximation (to study the emission probability).

The small variations observed in the shape and position of the BP are related to the changes in the distance of closest approach to the surface, which is determined for each type of surface and incidence condition, by the charge and mass of the projectile. Using a Molière potential [23] for H^+, He^+, Li^+, and C^{2+} on SnTe we obtain distances of closest approach of -1.7, -2.2, -2.4, -2.37 a.u., respectively.

In Fig. 3 we compare the calculation presented in Fig. 2 with the data published in Ref. [17]; we observe that the position of the maximun of the binary peaks are well described by the present model. On the other hand, to compare the shape and intensities it should be necessary to take into account the absolute experimental intensity after background substraction and correction for the transmission function of the analyzer.

2. Fermi energy and work function of the target

We show in Fig. 4 the binary electron energy distribution calculated for 0.98 MeV/amu Ar^{12+} colliding with several surfaces characterized by the Fermi energies E_F and work functions W listed in Table I. The incidence and observation angles are 1°. We can observe in Fig. 4 how these parameters affect the intensity, the width, and the position of the BP.

To our knowledge, the only available data to compare with our results are those measured by Ishikawa *et al.* [18], taken with the aim of analyzing the structure at E_M. There, the region of the binary peak was not considered in detail. The results are presented in the inset of Fig. 4. Even when the comparison is not straightforward it is possible to observe that the intensity of the BP depends on the target type.

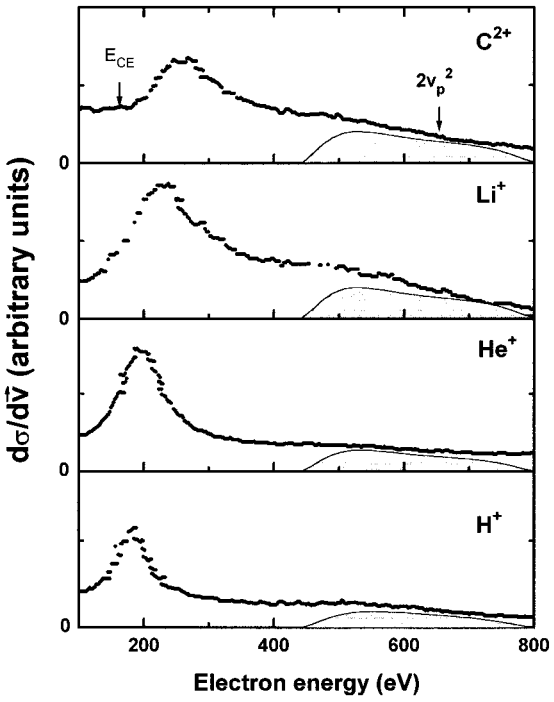

FIG. 3. Comparison between the calculations of Fig. 2 and the experimental data reported by Kimura *et al.* [17]. The arrows indicate the convoy electron energy E_{CE} and $2v_p^2$.

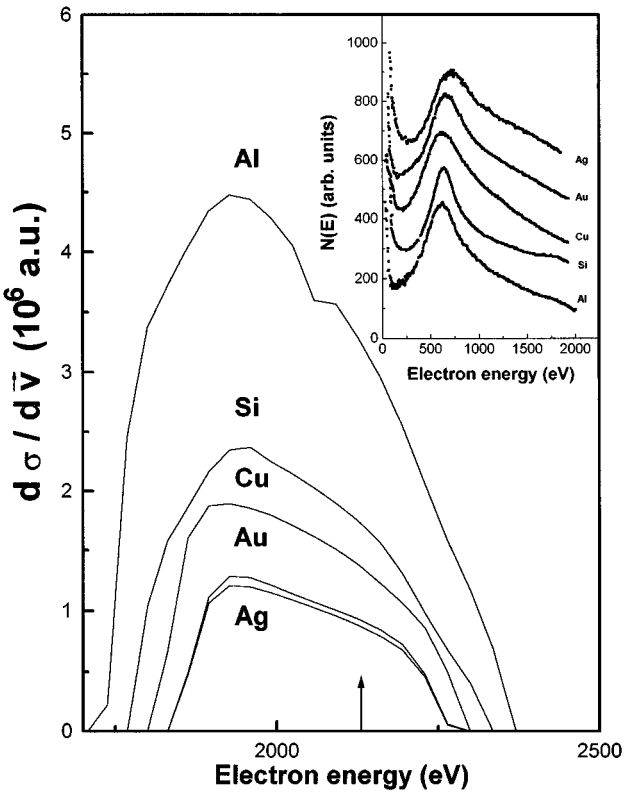

FIG. 4. Electron emission probability $d\sigma/d\vec{v}$ calculated for 0.98 MeV Ar^{12+} scattering from Al, Si, Cu, Au, and Ag surfaces with $\theta_i = 1°$ and $\theta_0 = 1°$. The arrow is at $2v_p^2$. The inset shows the experimental data measured by Ishikawa *et al.* [18].

3. Observation angles

We show in Fig. 5 the double differential cross section $d\sigma/d\vec{v}$ calculated for 0.98 MeV/amu Ar^{12+} scattering from an Al surface with $\theta_i = 1°$ and θ_0 equal to 3°, 6°, 8°, and 15°. As in the case of ion-atom collisions the maximum of the BP shifts to lower energies when the observation angles increases.

In the inset of Fig. 5 we present the available experimental data measured by Koyama [9]. The lines indicate the position of the maximum predicted by the present model. The position of the BP maximum at 15° is reasonably described by the model; for a detailed comparison with the experimental data it should be necessary to extend the spectra to higher electron energies.

TABLE I. Fermi energy, work function, and distance of closest approach used in the calculation shown in Fig. 4 for different target materials.

	Al	Si	Cu	Au	Ag
E_F (eV)	11.70	9.00	7.00	5.53	5.49
W (eV)	4.25	4.85	4.40	4.30	4.30
B (a.u.)	-4.14	-4.17	-3.41	-3.29	-3.04

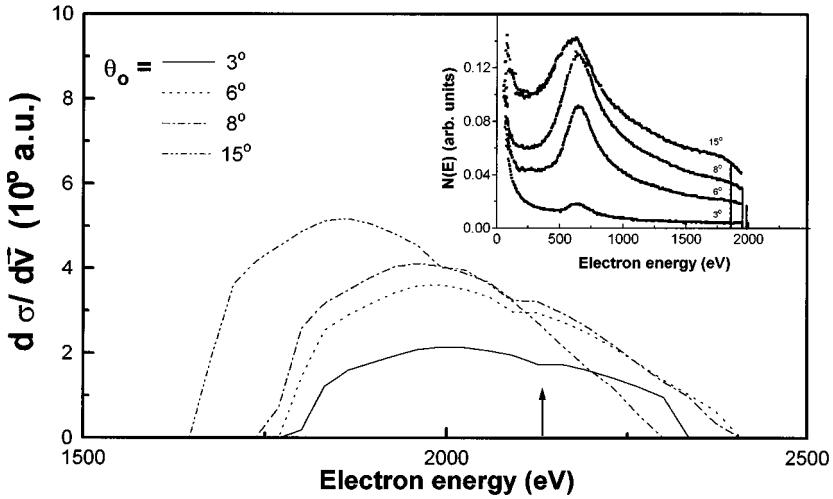

FIG. 5. Electron emission probability $d\sigma/d\vec{v}$ calculated for 0.98 MeV Ar^{12+} scattering from an Al surface with $\theta_i = 1°$ and the observation angles θ_0 indicated in the figure. The arrow is at $2v_p^2$. The inset shows the experimental data measured by Koyama [9] and the lines indicate the position of the maximum predicted by the present model.

B. The binary structure for low projectile energies

In Fig. 6 we present the electron emission probability $d\sigma/d\vec{v}$ calculated for 29 keV H^+ scattering from an Al surface with $\theta_i = 1.3°$ and $\theta_0 = 10°$. Three different cases are considered: (a) without screening, i.e., $a = 0.0$; (b) with a Thomas Fermi screening length $a = \sqrt{3}(\omega_p/v_F)$, with ω_p = bulk plasma frequency; and (c) similar to (b) but with ω_s (the surface plasma frequency) instead of ω_p since the characteristic range of the screened potential when the ion is outside the medium is related to the surface plasma frequency [4].

We observe in Fig. 6 that the binary peak cannot be identified as an independent structure of the spectrum as is the case for high projectile energies. In this case, the calculation of target ionization shows a low-energy structure that is strongly dependent on the screened potential. This behavior is related to the allowed final electron momentum, restricted by energy conservation [19]. If $|\mathbf{v}_p - \mathbf{k}_F| \leq \sqrt{2W}$ there will be no allowed final momentum states around $\mathbf{k}_f \simeq \mathbf{v}_p$ and then the electron emission probability has a maximum at low energy and a tail that extends up to an energy equal to $(k_f^M)^2/2$. The dependence of this effect on the electron observation angle is shown in Fig. 7, where we present the calculated double differential cross section $d\sigma/d\vec{v}$ for 29 keV H^+ scattering from an Al surface with $\theta_i = 1.3°$ and $\theta_0 = 10°$.

We show in Fig. 8 the electron emission probability $d\sigma/d\vec{v}$ for 30, 50, 70, and 100 keV H^+ scattering from an Al surface with $\theta_i = 1°$ and $\theta_0 = 1°$. The lines correspond to the calculations and the points to our experimental results. The experimental spectra are normalized with the incident current; the spectrum for 100 keV H^+ scattering from Al surface with $\theta_i = 1°$ and $\theta_0 = 30°$ was matched to the calculated curves at an electron energy of 230 eV. The same factor was used for all the spectra of Figs. 8 and 9.

As we have mentioned above, in the theoretical curves of Fig. 8 we observe that the BP appears as an independent structure only for sufficiently high projectile energy. This is because, for the case of H^+ scattering from Al, the condition $v_p \geq v_F + \sqrt{2V_0}$ is verified when the projectile energy is $>$ 100 keV.

The experimental spectra show the structures at E_{CE} and at E_M, as well as the low-energy structure mentioned above. An independent binary peak similar to that measured for the case of high projectile energy is not observed.

We can see from the comparison with the calculations that the present ionization mechanism cannot describe the structure at E_M. In particular, for 100 keV H^+ on Al this structure appears in the region where the final momentum states produced by a binary-encounter collision are forbidden by

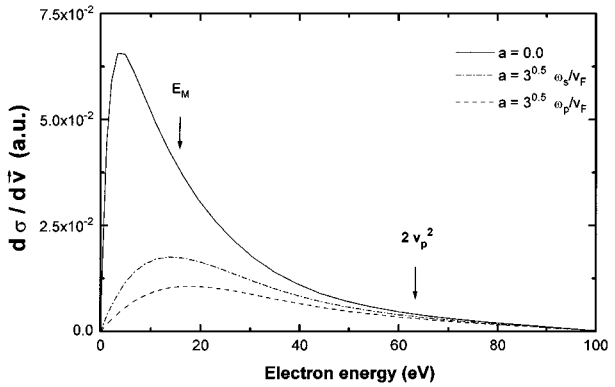

FIG. 6. Electron emission probability $d\sigma/d\vec{v}$ for 29 keV H^+ scattering from an Al surface with $\theta_i = 1.3°$ and $\theta_0 = 10°$. The curves correspond to the calculations done with the screening values **a** detailed in the figure. The arrows indicate the electron energy E_M and $2v_p^2$.

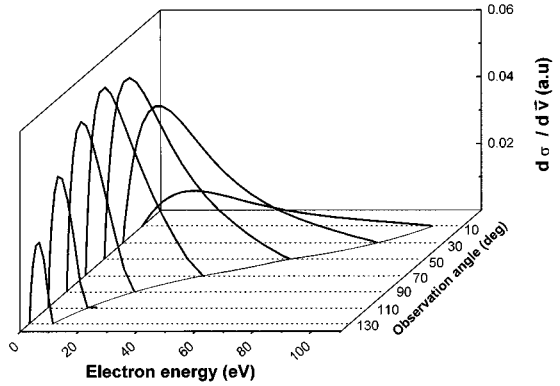

FIG. 7. Electron emission probability $d\sigma/d\vec{v}$ for 29 keV H^+ scattering from an Al surface with $\theta_i = 1.3°$ and the observation angles indicated in the figure.

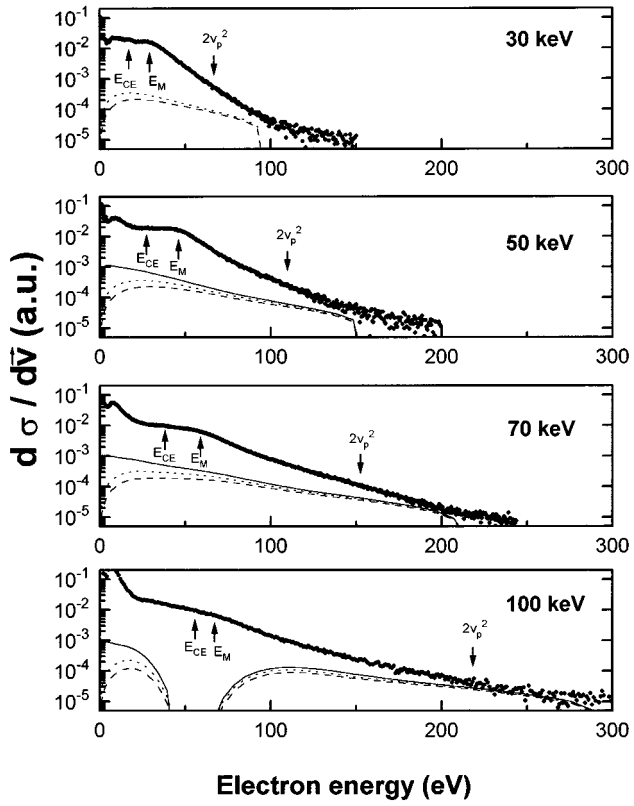

FIG. 8. Electron emission probability $d\sigma/d\vec{v}$ for 30, 50, 70, and 100 keV H^+ scattering from an Al surface with $\theta_i = 1°$ and $\theta_0 = 1°$. The lines correspond to the calculations done for the same screening values of Fig. 6 and the points to our experimental results. The arrows indicate the convoy electron energy E_{CE}, the structure at E_M, and $2v_p^2$.

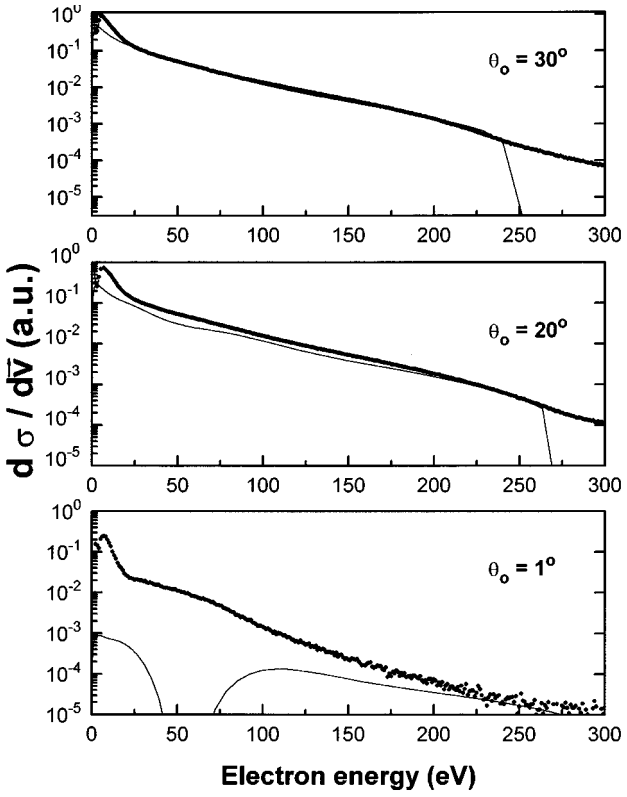

FIG. 9. Electron emission probability $d\sigma/d\vec{v}$ for 100 keV H^+ scattering from an Al surface with $\theta_i = 1°$ and the observation angles θ_0 indicated in the figure. The lines correspond to the calculations done with a screening value $a = 0$ and the points to our experimental results.

energy conservation laws. Within this model, the BP will contribute to the background of the structure at E_M and it will only determine the shape and the behavior of the high-energy tails.

In Fig. 9 we present the calculation and our experimental data obtained for 100 keV H^+ impinging on Al at 1° incidence for different observation angles. It can be seen that for high observation angles, where the convoy emission and the structure at E_M are almost suppressed, the present model describes qualitatively the whole electron spectra. A difference is observed in the low-energy part of the spectra, where the intensity of the experimental data is higher than that of the calculated ones. This discrepancy could be due to the following: (a) the screening potential—in this model we consider a direct ion-electron screened Coulomb interaction, approximated by a Yukawa-type potential; (b) simple electron-hole pair decay of surface and bulk plasmons; and (c) secondary-electron emission: primary electrons moving inside the solid can suffer multiples collisions, generating a collision cascade of secondary electrons that can be emitted from the surface. These last two effects were not taken into account in the present model and will produce an increment of the intensity in the low-energy region of the electron spectra.

V. CONCLUSIONS

In the case of high-energy collisions the electron energy spectrum presents a broad and relatively small structure in the high-energy region that coexists with the peak at E_M (Figs. 1–4). This structure, shifted to energies lower than $2v_p^2$, can be ascribed to ionization of the bulk due to direct collision with the impinging projectile (binary peak). The main characteristics of the BP at high projectile energies are the following.

(i) The shape and position of the maximum are hardly dependent on the charge and mass of the projectile (Figs. 2 and 3).

(ii) The position and intensity of the binary peak depend not only on the projectile velocity and the observation angle (Figs. 2 and 5) but also on the Fermi energy, work function, and density of states of the solid valence band. In particular, the shift to lower energies and the intensity are greater for higher surface barriers (Fig. 4 and Table I) and higher observation angles (Fig. 5).

For a thorough analysis of these behaviors it is necessary to acquire more experimental data in the BP region to show in detail its dependence on the parameters studied above. Furthermore, the effect of the electron transport and the inclusion of core electrons in the calculation of the ionization should be incorporated to the present model, especially for projectile incidence conditions in which the ion penetrates the topmost atomic layer of the solid.

In the case of intermediate projectile energies the calculations and the experimental data show that the binary peak does not appear as an independent structure on the electron spectra (Fig. 8). On the other hand, a high electron emission

is shown at low energies. The main characteristics of the electron emission at low projectile energies are summarized as follows.

(i) The position of the maximum and the intensity of the calculated spectra are strongly dependent on the screening factor (Fig. 6). For a better description of the low-energy region it would be necessary to take into account a more accurate theory [4].

(ii) Far off the direction of specular reflection of the projectile ($\theta_0 > 10°$), where the emission at E_M is strongly decreased, the present model is in good agreement with the experimental data (Fig. 9).

(iii) The electron emission produced by the direct screened Coulomb interaction between the projectile and the target electrons cannot account for the structure at E_M.

ACKNOWLEDGMENTS

We acknowledge partial support from CONICET (Grant No. PID 3292/92) and Fundación Balseiro.

[1] H. Winter, G. Dierkes, A. Hegmann, J. Leuker, H. W. Ortjahann, and R. Zimny, in *Ionization of Solids by Heavy Particles*, Vol. 306 of *NATO Advanced Stydy Institute, Series B: Physics*, edited by R. A. Baragiolo (Plenum, New York, 1993).

[2] C. Rau, N.J. Zheng, and M. Rösler, Nucl. Instrum Methods Phys. Res. Sect. B **78**, 247 (1993).

[3] M.L. Martiarena, E.A. Sánchez, O. Grizzi, and V.H. Ponce, J. Phys. C **5**, 285 (1993).

[4] F. J. García de Abajo and P. Echenique, Nucl. Instrum Methods Phys. Res. Sect. B **79**, 15 (1993).

[5] E.A. Sánchez, O. Grizzi, M.L. Martiarena, and V.H. Ponce, Phys. Rev. Lett. **71**, 801 (1993).

[6] P.A. Zeijlmans van Emmichoven, C.C. Havener, I.G. Hughes, D.M. Zehner, and F.W. Meyer, Phys. Rev. A **47**, 3998 (1993).

[7] A. Hegmann, R. Zimny, H.W. Ortjahann, H. Winter, and Z.L. Miskovic, Europhys. Lett. **26**, 383 (1994).

[8] M. Hasegawa, K. Kimura, and M. Mannami, J. Phys. Soc. Jpn. **57**, 1834 (1988).

[9] A. Koyama, Nucl. Instrum. Methods Phys. Res. Sect. B **67**, 103 (1992).

[10] K. Kimura, T. Kishi, and M. Mannami, Nucl. Instrum Methods Phys. Res. Sect. B **90**, 282 (1994).

[11] T. Iitaka, I.H. Ohtsuky, K. Hizawa, A. Koyama, and H. Ishikawa, Phys. Rev. Lett. **65**, 3160 (1990).

[12] C. Reinhold and J. Burgdörfer, Phys. Rev. Lett. **73**, 2508 (1994).

[13] N. Stoterfoht, in *Structure and Collisions of Ions and Atoms*, edited by I. Sellin, Topics in Current Physics Vol. 5 (Springer-Verlag, Berlin, 1978), p. 155.

[14] M. Landolt, R. Allenspach, and D. Mauri, J. Phys. D **57**, 3626 (1985).

[15] P.D. Fainstein, V.H. Ponce, and R.O. Rivarola, Phys. Rev. A **45**, 6417 (1992).

[16] A. González, P. Dahl, P. Hvelplund, and P.D. Fainstein, J. Phys. B **26**, L135 (1993).

[17] K. Kimura, M. Tsuji, and M. Mannami, Phys. Rev. A **46**, 2618 (1992).

[18] H. Ishikawa, A. Misu, K. Koyama, T. Iitaka, M. Uda, and Y. Ohtsuki, Nucl. Instrum. Methods Phys. Res. Sect. B **67**, 160 (1992).

[19] M.L. Martiarena, E.A. Sánchez, O. Grizzi, and V.H. Ponce, Nucl. Instrum. Methods Phys. Res. Sect. B **90**, 300 (1994).

[20] H. Bethe and Edwin Salpeter, *Quantum Mechanics of One- and Two-Electron Atoms* (Springer-Verlag, Berlin, 1957).

[21] R.E. Wilems, Ph.D. thesis, University of Tennessee, 1968 (unpublished).

[22] L.F. de Ferrariis, F. Tutzauer, E.A. Sánchez, and R.A. Baragiola, Nucl. Instrum. Methods Phys. Res. Sect. B **281**, 43 (1989).

[23] K. Kimura, M. Hasegawa, Y. Fujii, M. Susuki, and M. Mannami, Nucl. Instrum. Methods Phys. Res. Sect. B **33**, 358 (1988).